Comput Geosci (2017) 21:1023–1033
DOI 10.1007/s10596-017-9685-5

ORIGINAL PAPER

A finite volume scheme with improved well modeling in subsurface flow simulation

Vasiliy Kramarenko[1] · **Kirill Nikitin**[1,2] · **Yuri Vassilevski**[1,3]

Received: 17 October 2016 / Accepted: 30 June 2017 / Published online: 27 July 2017

Abstract We present the latest enhancement of the nonlinear monotone finite volume method for the near-well regions. The original nonlinear method is applicable for diffusion, advection-diffusion, and multiphase flow model equations with full anisotropic discontinuous permeability tensors on conformal polyhedral meshes. The approximation of the diffusive flux uses the nonlinear two-point stencil which reduces to the conventional two-point flux approximation (TPFA) on cubic meshes but has much better accuracy for the general case of non-orthogonal grids and anisotropic media. The latest modification of the nonlinear method takes into account the nonlinear (e.g., logarithmic) singularity of the pressure in the near-well region and introduces a correction to improve accuracy of the pressure and the flux calculation. In this paper, we consider a linear version of the nonlinear method waiving its monotonicity for sake of better accuracy. The new method is generalized for anisotropic media, polyhedral grids and nontrivial cases such as slanted, partially perforated wells or wells shifted from the cell center. Numerical experiments show noticeable reduction of numerical errors compared to the original monotone nonlinear FV scheme with the conventional Peaceman well model or with the given analytical well rate.

Keywords Finite volume scheme · Near-well correction · Well-driven flows · Improved well modeling

✉ Kirill Nikitin
nikitin.kira@gmail.com

Vasiliy Kramarenko
kramarenko.vasiliy@gmail.com

Yuri Vassilevski
yuri.vassilevski@gmail.com

[1] Institute of Numerical Mathematics of Russian Academy of Sciences, Moscow, Russia

[2] Nuclear Safety Institute of Russian Academy of Sciences, Moscow, Russia

[3] Moscow Institute of Physics and Technology, Dolgoprudny, Russia

1 Introduction

Cell-centered finite volume (FV) methods with the nonlinear flux discretization on cell faces attract growing attention in past few years [6]. An idea of the monotone schemes with nonlinear coefficients was suggested in [9] and further developed into a simple yet efficient monotone second-order method with the nonlinear two-point discretization of the diffusion and convection fluxes [3, 11, 12, 17]. Monotonicity of this method is understood in the sense of non-negativity of the discrete solution. The method was tested for the two- and three-phase black oil models [15] on conformal hexahedral meshes, polyhedral meshes produced by dynamic octrees [21] and by dynamic octrees with cut cells [16]. The later modification of the scheme combined the nonlinear flux approximation with the ideas from [1] (see also [20]) that assure the discrete maximum principle (DMP) and resulted in the nonlinear multi-point scheme with compact stencil [2, 7, 13]. Applications of the scheme with the DMP for two-phase flows were studied in [14].

The well model is the sensitive part of the black-oil simulator and has the major impact on calculated well rates. The solution in the near-well region is highly influenced by the well singularity. The idea to exploit that solution feature in the well model for FV schemes was suggested in

[4]. This approach was combined with the nonlinear FV scheme in [5] for the case of well-oriented prismatic grids in isotropic media. Our new method generalizes these ideas for anisotropic media, polyhedral grids, and arbitrary wells not necessarily adjusted neither with cells centers or with edges.

The key idea of the new near-well correction (NWC) method is to use a nonlinear (e.g., logarithmic) correction term for the reconstructed solution inside the flux discretization scheme in the near-well region. For the isotropic case, the linear-logarithmic reconstruction is used. The resulting method is exact on both linear and logarithmic solutions by construction and is generalized for the anisotropic media and for slanted wells. Since the method is applicable on arbitrary polyhedral grids, it requires no local grid refinement or any other grid modifications, which are widely used for modeling of areas with high pressure gradients [10]. Numerical experiments show the noticeable reduction of the numerical errors compared to the original monotone nonlinear FV scheme with the conventional Peaceman well model or with the given analytical well rate.

2 FV discretization scheme for diffusion problems

In order to introduce the numerical scheme, we consider the stationary diffusion equation.

Let Ω be a three-dimensional polyhedral domain with the Lipschitz boundary $\Gamma = \Gamma_N \cup \Gamma_D$. The diffusion equation for unknown pressure p with the Dirichlet or Neumann boundary conditions is written in the mixed form:

$$\begin{aligned} \mathbf{q} = -\mathbb{K}\nabla p, \qquad \operatorname{div} \mathbf{q} &= f \quad \text{in } \Omega, \\ p &= g \quad \text{on } \Gamma_D, \\ \mathbf{q}\cdot\mathbf{n} &= 0 \quad \text{on } \Gamma_N. \end{aligned} \tag{1}$$

Here, $\mathbb{K}(\mathbf{x})$ is a symmetric positive definite (possibly anisotropic) diffusion tensor, $f(\mathbf{x})$ is a source term, $g(\mathbf{x})$ is a given Dirichlet data for the Dirichlet part of the boundary Γ_D.

The cell-centered FV scheme uses one degree of freedom per cell T, p_T, collocated at cell barycenter $\mathbf{x}_T$. Integrating the mass balance Eq. 1 over T and using the divergence theorem, we obtain:

$$\sum_{f\in\partial T} \sigma_{T,f}\, q_f = \int_T f \,\mathrm{d}x, \qquad q_f = \int_f \mathbf{q}\cdot\mathbf{n}_f \,\mathrm{d}S, \tag{2}$$

where q_f is the normal flux across the face f, and $\sigma_{T,f}$ is either 1 or -1 depending on the mutual orientation of the unit normal vectors $\mathbf{n}_f$ and $\mathbf{n}_T$ ($\mathbf{n}_T$ denotes the outward normal vector for T).

Two nonlinear schemes for the flux (2) discretization were suggested in [11, 13] for 2D and [2, 3] 3D case. In this work, we present a linear multi-point scheme that shares similar construction principles.

3 Nonlinear near-well correction method

Consider a near-well region which spans well singularity (see Fig. 1). The key idea of the method follows [4, 5]. We modify the nonlinear monotone FV scheme from [3] and take into account the solution singularity near an isolated well. In contrast to [5], our method is designed for anisotropic media, arbitrary polyhedral cells, and arbitrary well location.

In the original nonlinear FV method, the discrete fluxes are calculated on the basis of the piecewise linear reconstruction of the unknown field. The NWC method takes into account the nonlinearity of the solution near the specific object such as the well.

We consider the pressure field to be the sum of linear and nonlinear functions for each cell in a near-well region:

$$p_T = \underbrace{a\,x + b\,y + c\,z + d}_{p_{lin}} + \underbrace{e\,F(x,y,z)}_{p_F}, \tag{3}$$

where $F(x, y, z)$ is a function representing the singularity.

The finite volume discretization requires the normal component of the flux $\mathbf{q} = -\mathbb{K}\nabla p$ to be integrated on each face f of T:

$$\begin{aligned} \int_f \mathbf{q}\cdot\mathbf{n}_f \mathrm{d}S &= -\int_f (\mathbb{K}\nabla p_T)\cdot\mathbf{n}_f \mathrm{d}S \\ &= -\int_f (\mathbb{K}\nabla p_{lin})\cdot\mathbf{n}_f \mathrm{d}S - \int_f (\mathbb{K}\nabla p_F)\cdot\mathbf{n}_f \mathrm{d}S. \end{aligned} \tag{4}$$

Combining (3) and (4) yields the mean normal flux

$$\begin{aligned} q_f &= \int_f \mathbf{q}\cdot\mathbf{n}_f \mathrm{d}S \\ &= -\int_f \mathbb{K}\begin{pmatrix} a \\ b \\ c \end{pmatrix}\cdot\mathbf{n}_f \mathrm{d}S - e\int_f (\mathbb{K}\nabla F(x,y,z))\cdot\mathbf{n}_f \mathrm{d}S \\ &= a\ell_1 + b\ell_2 + c\ell_3 + e\ell_4. \end{aligned} \tag{5}$$

In the following, we shall omit index f whenever it does not result in confusion.

Integrals for ℓ_1, ℓ_2, and ℓ_3 are calculated exactly. Integral for ℓ_4 can also be calculated exactly for some simple

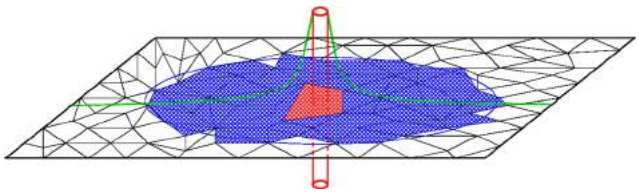

Fig. 1 Logarithmic singularity in the near-well region

cases of well, grid and tensor (see [5]), but for more general cases the numerical integration should be used (see Section 4). The coefficients ℓ_i depend solely on the mesh and problem data, and are calculated explicitly, while the coefficients (a, b, c, e) are recovered from the solution at the neighboring cells.

Let T_+ and T_- be neighboring cells sharing a face f, $\mathbf{x}_+$, $\mathbf{x}_-$ denote centroids of these cells. We take four points $\mathbf{x}_i$ ($\mathbf{x}_i \neq \mathbf{x}_+$) and call four vectors $\mathbf{t}_i = \mathbf{x}_i - \mathbf{x}_+$ the *quadruplet*. Points $\mathbf{x}_i$ denote centers of the neighboring cells or faces of T, $p_i = p(\mathbf{x}_i)$ and $p_+ = p(\mathbf{x}_+)$.

We assume the same representation (3) for vectors of each quadruplet, which gives us:

$$\begin{pmatrix} p_1 - p_+ \\ p_2 - p_+ \\ p_3 - p_+ \\ p_4 - p_+ \end{pmatrix} = \begin{bmatrix} x_1 - x_+ & y_1 - y_+ & z_1 - z_+ & F_1 - F_+ \\ x_2 - x_+ & y_2 - y_+ & z_2 - z_+ & F_2 - F_+ \\ x_3 - x_+ & y_3 - y_+ & z_3 - z_+ & F_3 - F_+ \\ x_4 - x_+ & y_4 - y_+ & z_4 - z_+ & F_4 - F_+ \end{bmatrix} \begin{pmatrix} a \\ b \\ c \\ e \end{pmatrix}, \tag{6}$$

where $F_* = F(x_*, y_*, z_*)$.

The collocation points of the quadruplet should be chosen carefully in order to avoid degenerated matrix in (6). Our algorithm for quadruplet points selection is as follows:

Algorithm 1 Quadruplet points selection

1: Select the first point $\mathbf{x}_1 = \mathbf{x}_-$
2: Compose set Σ of all neighboring points of $\mathbf{x}_+$, $\mathbf{x}_i \neq \mathbf{x}_-$
3: **for** every three different points $\mathbf{x}_2, \mathbf{x}_3, \mathbf{x}_4$ from Σ **do**
4: Compute determinant of the quadruplet matrix (6)
5: **end for**
6: **if** all quadruplets have degenerate matrix (6) **then**
7: Add more points to the set Σ
8: goto 3
9: **end if**
10: Choose quadruplet with the largest matrix determinant

Solving the system (6) with the largest matrix determinant provides us the coefficients a_+, b_+, c_+, e_+ for the cell T_+:

$$a_+ = \sum_j (p_j - p_+)\, m_{1,j}, \qquad b_+ = \sum_j (p_j - p_+)\, m_{2,j},$$
$$c_+ = \sum_j (p_j - p_+)\, m_{3,j}, \qquad e_+ = \sum_j (p_j - p_+)\, m_{4,j}, \tag{7}$$

where $m_{i,j}$ are the elements of the inverse matrix from (6). Taking T_- instead of T_+ and considering $-\mathbf{q} \cdot \mathbf{n}_f$ provides us the second flux approximation.

Applying (7) to Eq. 5 gives us

$$\begin{aligned} q_\pm &= \pm \int_f \mathbf{q} \cdot \mathbf{n}_f \mathrm{d}S \\ &= \pm \Big[\ell_1 \sum_j (p_j - p_\pm)\, m^\pm_{1,j} + \ell_2 \sum_j (p_j - p_\pm)\, m^\pm_{2,j} \\ &\quad + \ell_3 \sum_j (p_j - p_\pm)\, m^\pm_{3,j} + \ell_4 \sum_j (p_j - p_\pm)\, m^\pm_{4,j} \Big], \end{aligned} \tag{8}$$

or

$$\begin{aligned} q_\pm &= \pm \Big[\sum_j p_j \underbrace{\sum_i \ell_i\, m^\pm_{i,j}}_{k^\pm_j} - p_\pm \sum_j \underbrace{\sum_i \ell_i\, m^\pm_{i,j}}_{k^\pm_j} \Big] \\ &= \pm \Big(\sum_j k^\pm_j\, (p_j - p_\pm) \Big). \end{aligned} \tag{9}$$

The resulting flux approximation is obtained as the weighted sum of q_+ and q_- with coefficients $\mu_+ + \mu_- = 1$

$$q_f = \mu_+ \Big(\sum_j k^+_j\, (p_j - p_+) \Big) - \mu_- \Big(\sum_{j'} k^-_{j'} \cdot (p_{j'} - p_-) \Big). \tag{10}$$

To construct the *linear* multi-point flux discretization, we considered $\mu_+ = \mu_- = 1/2$. One may also construct a nonlinear scheme (similar to [2, 3]) using pressure-dependant coefficients, but this is the subject for a future study.

4 Numerical issues of implementation

4.1 Well cell model

The near-well correction method replaces the conventional Peaceman well model from [18] and is applicable to the cases of arbitrary polyhedral cells, slanted wells and wells separated from grid cell centers.

The original Peaceman formula was derived on the basis of two key assumptions:

- The well flux is compensated by the sum of the *linear* flux approximations for the well cell faces,
- It is considered for the perfect vertical well where all the neighboring cells pressures are given by the Dupuit formula to catch the logarithmic behavior of the solution in the near-well region.

These assumptions require selection of an equivalent radius, which is used for definition of the well cell pressure and ensures flux continuity.

In contrast to the Peaceman approach, the new well model is incorporated in the near-well correction scheme which takes the singularity into account by construction

and does not impose additional restrictions on the well cell degree of freedom.

The new approach allows us to consider the general case of the well not passing through the cell center. For each well cell, we introduce an additional point on the well segment associated with the bottom hole pressure. Using this point and considering only outer flux ($\mu_+ = 1, \mu_- = 0$) in (10), we get an additional relation for the facial fluxes of the well cell. Therefore, for the well cell faces, we have two flux approximations with different stencils (see Fig. 2). For each quadruplet calculation, the points inside the well are projected to the well surface in order to avoid the singularity.

Summarizing fluxes for the well cell gives us the well cell equation:

$$\sum_f \left[\frac{1}{2}\Big(\sum_j k_j^+ (p_j - p_+) \Big) - \frac{1}{2}\Big(\sum_{j'} k_{j'}^- (p_{j'} - p_-) \Big) \right] = \sum_f \left(\sum_l k_l^+ (p_l - p_w) \right). \quad (11)$$

If we use the given well flux q_w condition, an additional equation for unknown p_w will occur:

$$\sum_{\text{well cells}} \sum_f \Big(\sum_l k_l^+ (p_l - p_w) \Big) = q_w. \quad (12)$$

4.2 Isotropic case

The particular choice of singularity function F in (3) depends on geometric and physical assumptions. A perfect well in isotropic media allows us to use the Dupuit formula, providing $F(x, y, z) = ln(r)$, where $r(x, y, z)$ is the distance to the well axis.

4.3 Anisotropic case

The 2D anisotropic case with $\mathbb{K} = diag(k_x, k_y)$ and $k_y > k_x$ is considered in [19] where the singularity function is the solution of the isolated perfect well problem. The main steps of derivation of F in this case are as follows.

First, the space transformation is applied:

$$x' = \left(\frac{k_y}{k_x}\right)^{0.25} x, \qquad y' = \left(\frac{k_x}{k_y}\right)^{0.25} y, \quad (13)$$

and the new coordinates are transformed to the elliptic ones:

$$x' = B \cosh(\rho) \cos(\phi), \qquad y' = B \sinh(\rho) \sin(\phi), \quad (14)$$

where $B = \sqrt{r_w^2 (k_y - k_x)/(k_x k_y)^{1/2}}$ is the coefficient suggested in [19] and r_w is the well radius.

In coordinates (ρ, ϕ), the analytical solution is:

$$p = p_w - \frac{q_w}{2\pi\sqrt{k_x k_y}} (\rho - \rho_w). \quad (15)$$

The elliptic coordinate ρ is expressed from (14) as:

$$\rho = \operatorname{arcosh} \sqrt{\frac{\sqrt{x'^2 + (y' - B)^2} + \sqrt{x'^2 + (y' + B)^2}}{4B^2}} \quad (16)$$

The singularity function $F(x, y, z)$ is given by (16). The integral ℓ_4 in (5) is calculated by the numerical integration over the face with a high order quadrature formula

$$\ell_4 = -\int_f \mathbb{K}\nabla F(x, y, z) \cdot \mathbf{n}_f \mathrm{d}S = -\int_f \mathbf{v} \cdot \mathbf{n}_f \mathrm{d}S. \quad (17)$$

Here, vector $\mathbf{v} = \mathbb{K}\nabla F(x, y, z)$ is given in the elliptic coordinates:

$$\mathbf{v} = \begin{pmatrix} v_x \\ v_y \end{pmatrix} = \begin{pmatrix} \frac{k_x \sqrt[4]{\frac{k_y}{k_x}} \sinh\rho \cos\phi}{B(\sinh^2\rho + \sin^2\phi)} \\ \frac{k_y \sqrt[4]{\frac{k_x}{k_y}} \cosh\rho \sin\phi}{B(\sinh^2\rho + \sin^2\phi)} \end{pmatrix}. \quad (18)$$

In the 3D case, the permeability tensor may be full anisotropic and the well may be not aligned with the grid and/or tensor axes. Under assumption of the infinite well, we consider the analytical solution to be pseudo-2D in the plane orthogonal to the well (see Fig. 3) with a corresponding 2D tensor $\mathbb{K}'_{xy} = diag(k'_x, k'_y)$ recovered by the following algorithm:

Algorithm 2 Construction of $\mathbb{K}'_{xy}$

1: Apply coordinate rotation which makes the well vertical
2: Calculate tensor $\mathbb{K}'$ in the rotated coordinates
3: Take the 2×2 leading submatrix of the tensor corresponding to directions orthogonal to the well
4: Diagonalize the 2×2 submatrix to obtain k'_x and k'_y

The 2D tensor $\mathbb{K}'_{xy}$ can now be used in the appropriate coordinate system to derive the analytical solution (15) and

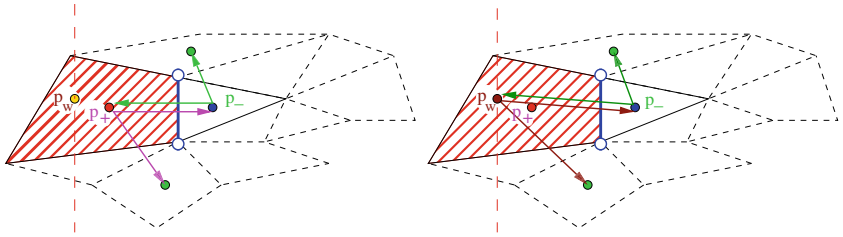

Fig. 2 Well cell: stencils for the reservoir pressure (*left*) and the additional well pressure (*right*)

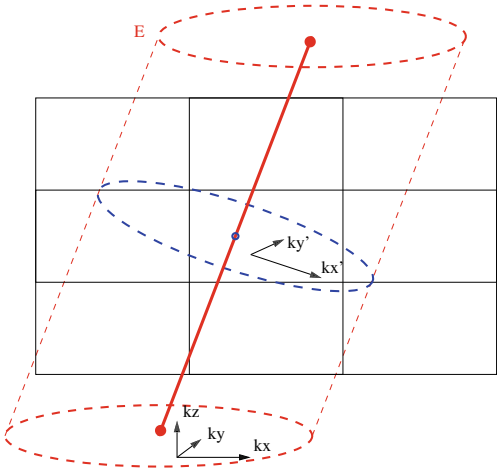

Fig. 3 Slanted well in anisotropic media

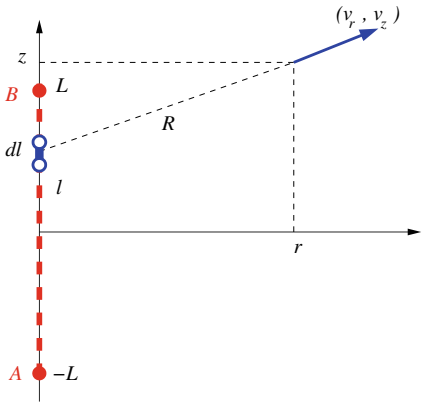

Fig. 4 Flux from the infinitesimal part of the well segment

solution gradient (18). The integral ℓ_4 is calculated similarly to (17) by a high order quadrature formula in 3D.

4.4 Partially perforated well

In real world applications, no well is perfect due to the finite length of the perforation. In this case, the exact solution for the finite perforation segment may be used.

Consider the line segment $[A, B]$ with the uniform flux density $q/2L$ in isotropic media, $\mathbb{K} = k\mathbb{I}$, $A = (0, 0, -L)$, $B = (0, 0, L)$. One can consider each point of segment as a point source. The flux from this point can be represented as a uniform flux from infinitesimal part of the segment $\Delta q = q\,\Delta l/2L$. Darcy flux at distance R is directed away from the segment and has the following magnitude [8]:

$$|\Delta \mathbf{u}| = \frac{\Delta q}{4\pi}\,\frac{1}{R^2}. \tag{19}$$

If we consider a point at distance r to the well line and at height z from the midpoint of the well segment, the distance R from an infinitesimal part of the segment will be

$$R = \sqrt{r^2 + (z-l)^2}, \tag{20}$$

where l is the distance from the midpoint of the well segment to this part (see Fig. 4).

The components of $\Delta\mathbf{u} = (\Delta u_r, \Delta u_z)^T$ at the point (r, z) are:

$$\Delta u_r = |\Delta \mathbf{u}|\,\frac{r}{R}, \qquad \Delta u_z = |\Delta \mathbf{u}|\,\frac{z-l}{R}. \tag{21}$$

The flux $\mathbf{v}(r, z) = (v_r, v_z)^T$ at the point (r, z) is the sum of contributions from each infinitesimal part of the well segment. Integrating (21) over the segment $[A, B]$, we obtain:

$$\begin{aligned} v_r &= \int_{-L}^{L} \frac{q\,r}{8L\,\pi\,R^3}dl = \frac{q}{8L\,\pi}\,\frac{l-z}{r\sqrt{r^2+(z-l)^2}}\Bigg|_{-L}^{L} \\ &= \frac{q}{8L\,\pi}\left(\frac{L-z}{r\sqrt{r^2+(z-L)^2}} + \frac{L+z}{r\sqrt{r^2+(z+L)^2}}\right), \\ v_z &= \int_{-L}^{L} \frac{q\,(z-l)}{8L\,\pi\,R^3}dl = \frac{q}{8L\,\pi}\,\frac{1}{\sqrt{r^2+(z-l)^2}}\Bigg|_{-L}^{L} \\ &= \frac{q}{8L\,\pi}\left(\frac{1}{\sqrt{r^2+(z-L)^2}} - \frac{1}{\sqrt{r^2+(z+L)^2}}\right). \end{aligned} \tag{22}$$

Now, we search for a smooth field $p(r, z)$ such that $-k\nabla p = \mathbf{v}(r, z)$. Integration of (22) provides us the pressure field:

$$p = C - F(r, z), \tag{23}$$

with the singularity function:

$$\begin{aligned} F(r, z) = \frac{q}{8\,L\pi\,k}\,[&2\ln r \\ &- \ln\left(\sqrt{r^2+(L-z)^2} + (L-z)\right) \\ &- \ln\left(\sqrt{r^2+(L+z)^2} + (L+z)\right)\Big]. \end{aligned} \tag{24}$$

Table 1 Flux and solution error for the NFV and the NWC methods for shifted well on the uniform rectangular grid $33 \times 33 \times 1$

δ	$\varepsilon^{NFV}_{p,anl}$	$\varepsilon^{NWC}_{p,anl}$	$\varepsilon^{NFV}_{p,pcm}$	ε^{NWC}_{p}	ε^{NFV}_{q}	ε^{NWC}_{q}
0	1.4e–4	1.3e–11	1.8e–4	1.3e–11	5.0e–3	8.9e–11
0.1	1.5e–3	6.3e–12	1.5e–3	1.5e–11	5.0e–3	1.2e–10
0.3	5.6e–4	2.3e–11	5.8e–4	2.0e–11	5.0e–3	4.7e–10
0.5	7.1e–4	2.7e–11	7.1e–4	2.1e–11	5.0e–3	4.9e–10
0.7	1.1e–3	5.2e–11	1.1e–3	1.1e–11	5.0e–3	1.5e–9

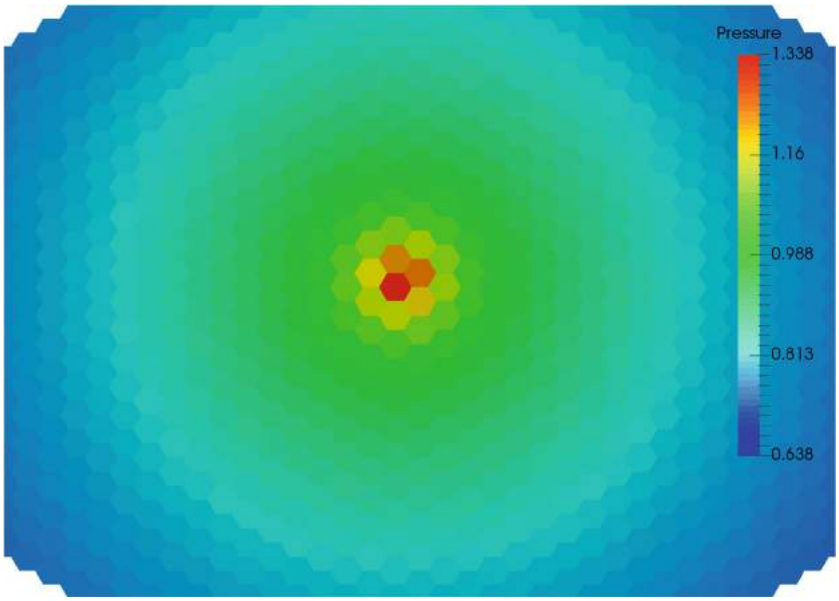

Fig. 5 Solution for the NWC scheme and the new well cell model for shifted well on hexagonal prismatic grid, $\delta = 0.5$

The constant C can now be expressed via the pressure p_w fixed on the well surface at a point with local coordinates $(r_w, 0)$. The final analytical pressure of the isolated partially perforated well is the following:

$$p = p_w - \frac{q}{8\,L\,\pi\,k}\left[\ln\frac{r^2}{L_-\,L_+} - \ln\frac{r_w^2}{L+\sqrt{r_w^2+L^2}}\right], \tag{25}$$

where $L_\pm = L \pm z + \sqrt{r^2 + (L \pm z)^2}$.

The solution (25) may be used in (3) for correction of the fluxes in the near-well region.

We note that for $L \to \infty$, $F(r, z)$ tends to the solution for the perfect well.

5 Numerical experiments

In order to test our approach, we study it on analytical solutions. We consider 2D isotropic case with a shifted well on cubic and hexagonal prismatic grids, 3D isotropic case with slanted and partially perforated wells, 2D and 3D cases with highly anisotropic media, and 2D case with two vertical wells.

All variables used in experiments are nondimensional: the well rate is 1 and the bottom hole pressure is 2. These two parameters provide the analytical solution around the well. The Dirichlet condition for known analytical solution is set on the domain boundary.

The computational domain sizes are $100 \times 100 \times 3$ for the vertical well and $100 \times 100 \times 12.5$ for the slanted and partially perforated wells, the well radius $r_w = 0.01$, the permeability tensor is a diagonal matrix $\mathbb{K} = diag(k_x, k_y, k_y)$. We consider different horizontal anisotropy ratios k_y/k_x. For 2D cases, we consider a pseudo-2D domain: grid dimensions are $N \times N \times 1$ with the no-flow conditions of the top and the bottom boundaries.

In our experiments, we consider two scenarios:

1. An analytical rate for the well cell is given. This allows us to compare the nonlinear monotone FV scheme (NFV) and the new near-well correction (NWC) scheme without the influence of the well cell model. For this scenario, we compute relative L^2 errors norms for the pressure field compared to the known analytical solution: $\varepsilon_{p,anl}^{NFV}$ and $\varepsilon_{p,anl}^{NWC}$.
2. The well cell model for a given bottom hole pressure is applied. The Peaceman formula is applicable only for

Table 2 Solution error for the NFV and the NWC methods for shifted well on hexagonal prismatic grid

δ	$\varepsilon_{p,anl}^{NFV}$	ε_{p}^{NWC}
0	1.1e–4	8.2e–11
0.1	1.4e–3	2.0e–11
0.3	4.2e–3	1.0e–11
0.5	7.1e–3	1.1e–11

Table 3 Flux and solution error for the NFV and the NWC methods for anisotropic case on non-orthogonal $N \times N \times 1$ grids with $N = 67$

k_y/k_x	$\varepsilon_{p,anl}^{NFV}$	ε_{p}^{NWC}	$\varepsilon_{2p,anl}^{NFV}$	ε_{2p}^{NWC}	ε_{q}^{NWC}
10	5.3e–4	1.9e–9	5.6e–2	2.0e–7	4.7e–7
100	1.7e–4	9.0e–9	5.9e–2	2.7e–6	1.3e–5
1000	9.0e–4	7.0e–8	8.0e–2	6.2e–5	6.6e–4
10000	4.0e–5	5.7e–8	1.1e–1	1.5e–3	1.7e–3

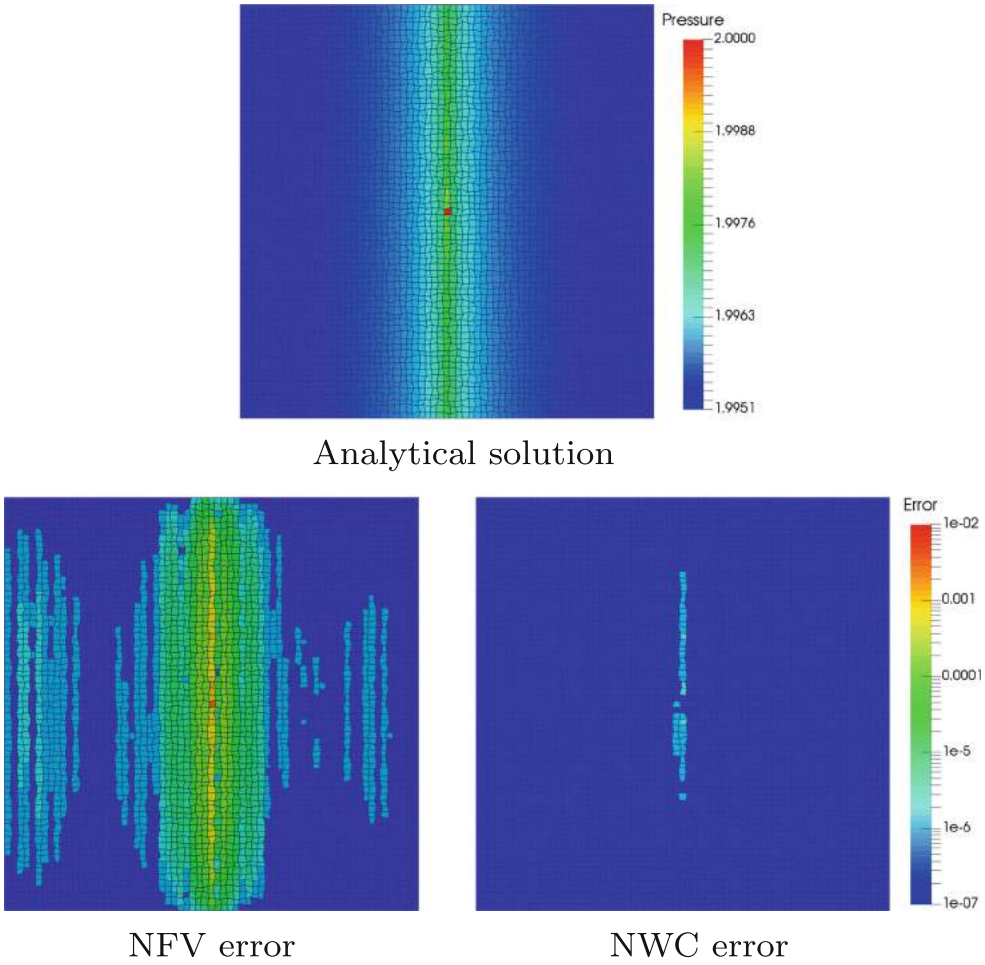

Fig. 6 Analytical solution (*top*) and solution errors for the NFV (*bottom-left*) and the NWC (*bottom-right*) methods for anisotropic case $k_y/k_x = 10{,}000$ on non-orthogonal grid with $N = 67$

cubic grids and is used with the nonlinear monotone scheme [15], while the new well cell model is used for all experiments in combination with the NWC scheme. In this case, we compute both relative L^2 error norms for the pressure ($\varepsilon_{p,pcm}^{NFV}$ and ε_p^{NWC}) and the well rate errors (ε_q^{NFV} and ε_q^{NWC}).

5.1 2D isotropic case, shifted well

We consider a cubic grid with a vertical well shifted from the well cell centroid. The well is shifted along the diagonal of the domain by the value $\delta d/2$, where d is the cell diagonal length. The analytical solution for $\mathbb{K} = \mathbb{I}$ is:

$$p = p_w - \frac{q_w}{2\pi h_w} \ln \frac{r}{r_w}, \tag{26}$$

where $r = \sqrt{(x - \delta d/2)^2 + (y - \delta d/2)^2}$.

By construction, any well index-based method incorporating the well within a single cell, will not provide the non-symmetric solution. In contrast, the new well cell model can reproduce a non-symmetric solution.

Table 4 Solution error for the NFV and the NWC methods, and the flux error for the NWC method. 3D isotropic case with ten layers for the slanted well

α	$\varepsilon_{p,anl}^{NFV}$	ε_p^{NWC}	ε_q^{NWC}
0°	6.5e–4	1.0e–12	3.0e–11
30°	1.2e–4	3.6e–9	3.1e–4
45°	1.7e–4	3.7e–12	1.3e–4
60°	1.1e–4	1.7e–10	7.5e–7

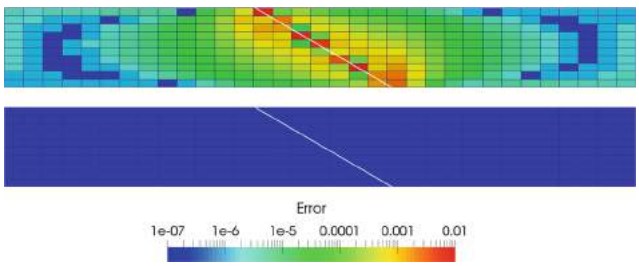

Fig. 7 Solution error for $\alpha = 60°$ for the NFV (*top*) and the NWC (*bottom*) methods. 3D isotropic case with ten layers for the slanted well

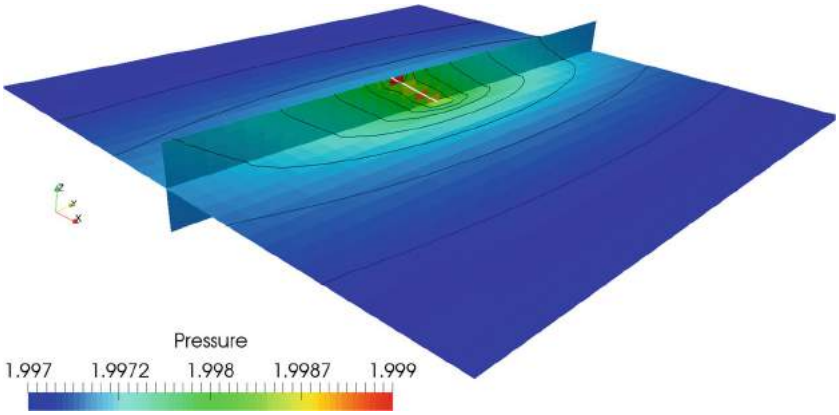

Fig. 8 Analytical solution for $\alpha = 60°$ for 3D anisotropic case with ten layers for the slanted well, $\mathbb{K} = diag\{10, 100, 1\}$

For the sake of comparison, we apply the Peaceman cubic grid formula with NFV method. Table 1 presents the numerical errors for the shifted well on the uniform rectangular grid $33 \times 33 \times 1$: the relative error L^2-norms for the NFV and the NWC schemes with the analytical well cell rates, the relative error L^2-norm and the well rate error for the NWC method coupled with the new well cell model. One can see that the NWC scheme is exact for the shifted isolated perfect well.

We also considered the similar problem on a hexagonal prismatic grid. Figure 5 presents the computational grid and the non-symmetric solution for the NWC method. The domain is not a parallelepiped in this case and the boundaries are approximated by faces of hexagonal prisms. Table 2 shows the relative L^2-norms of pressure error for the NFV scheme with the analytical well cell rate and for the NWC method coupled with the new well cell model.

5.2 2D anisotropic case, non-orthogonal grid

The next example uses a non-orthogonal grid constructed from the uniform rectangular grid by shifting nodes while keeping the cell faces planar. We consider high anisotropy cases with $k_x = 1$, $k_y = 10, 100, 1000, 10{,}000$ for different grid sizes N along horizontal axes. The analytical solution is given by (15) and (16).

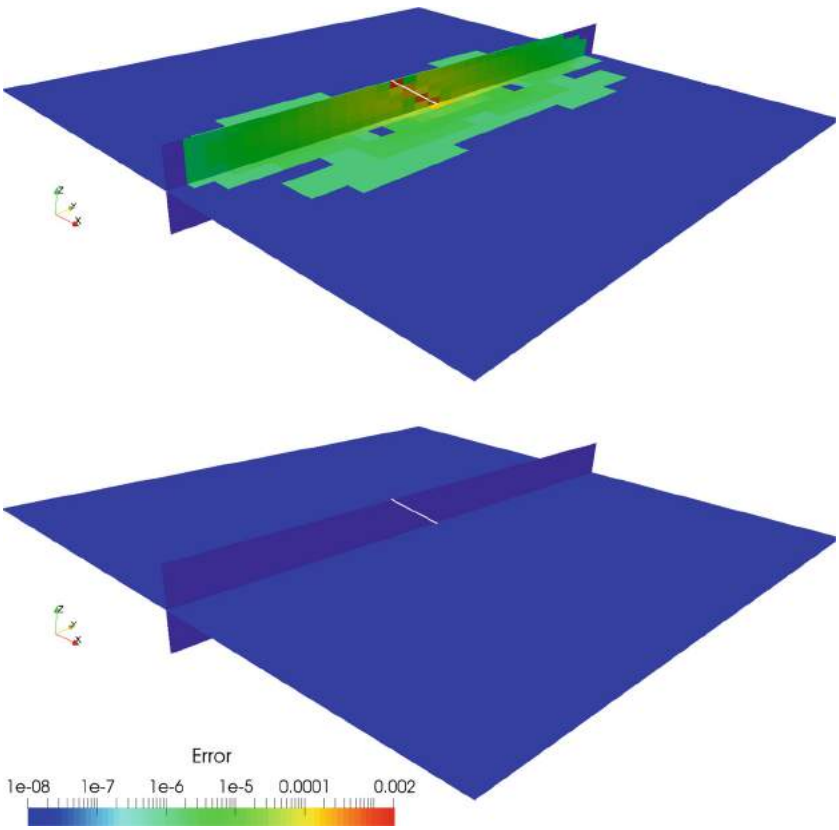

Fig. 9 Solution error for $\alpha = 60°$ for the NFV (*top*) and the NWC (*bottom*) methods. 3D anisotropic case with ten layers for the slanted well, $\mathbb{K} = diag(10, 100, 1)$

Table 5 Solution error for the NFV and the NWC methods, and the flux error for the NWC method. 3D anisotropic case for the slanted well, $\mathbb{K} = diag(10, 100, 1)$

α	$\varepsilon_{p,anl}^{NFV}$	ε_{p}^{NWC}	$\varepsilon_{2p,anl}^{NFV}$	ε_{2p}^{NWC}	ε_{q}^{NWC}
0°	2.5e–5	2.8e–11	1.2e–1	1.3e–7	4.9e–7
30°	5.9e–6	1.7e–10	2.4e–2	8.6e–7	1.0e–5
45°	5.6e–6	2.2e–10	2.6e–2	1.0e–6	9.0e–6
60°	3.8e–6	2.5e–10	1.9e–2	1.2e–6	2.9e–5

Flux and solution errors for the NFV and the NWC methods are compared in Table 3 for different anisotropy ratios. Due to the high anisotropy, the solution variation is very small: $p \in [1.995,\ 2.0]$ for $k_y/k_x = 10{,}000$. To capture the error compared to this variation, we introduce ε_{2p}, the relative error normalized by $||p_{anl} - p_{anl,min}||$ instead of $||p_{anl}||$. Since the Peaceman method is not applicable for this case, we can present only the NWC method flux error ε_q^{NWC}. The latter is the absolute (not relative) error and one can see that the calculated flux error is small even for the extremely high anisotropy.

Solution errors for both methods on the non-orthogonal grid $N \times N \times 1$, $N = 67$, are presented in Fig. 6.

5.3 3D case, slanted well

In the 3D case, we consider the domain with the hexahedral orthogonal grid and a slanted (not vertical) well. The grid has ten layers and Dirichlet boundary conditions are given for all boundaries. For the isotropic case, the analytical solution is given by formula (26) with r being the distance from the point to the well.

The error dependence on the well tilt angle for the NFV and the NWC methods are presented in Table 4. Angle $\alpha = 0°$ denotes to the vertical well. Vertical cross-section of the grid with the error fields for $\alpha = 60°$ for the NFV and the NWC methods are presented in Fig. 7 (top) and Fig. 7 (bottom), respectively.

For the anisotropic case, we consider the similar experiment layout with anisotropic tensor $\mathbb{K} = diag(10, 100, 1)$. The analytical solution for each cutplane orthogonal to the well axis is given by (15) and (16) with the corresponding 2D tensor $\mathbb{K}'_{xy} = diag(10, 100\cos\alpha + \sin\alpha)$.

Figure 8 shows two cross-sections of the analytical solution for this case. Errors for the NFV and the NWC methods are presented in Fig. 9 and in Table 5. By analogy with the anisotropic case from Section 5.2, we calculate $\varepsilon_{2p,anl}^{NFV}$ and ε_{2p}^{NWC} to show the real magnitude of the error compared to the solution variation.

One can see that the solution error for the method without nonlinear correction is noticeable compared to the solution variation (see $\varepsilon_{2p,anl}^{NFV}$) while the NWC method produces almost zero error. The numerical flux error ε_q^{NWC} is also small for the considered anisotropy ratio.

5.4 3D isotropic case, partially perforated well

The partially perforated well case repeats the previous test case layout with the reservoir dimensions $100 \times 100 \times 12.5$. The well perforation is a vertical finite segment $[A, B]$, where $A = (50, 50, 1.95)$ and $B = (50, 50, 10.55)$. The permeability tensor is scalar, $\mathbb{K} = \mathbb{I}$. For the analytical solution, we use (25).

Figure 10 (top) presents the vertical cross-section of the grid with the analytical solution for the partially perforated

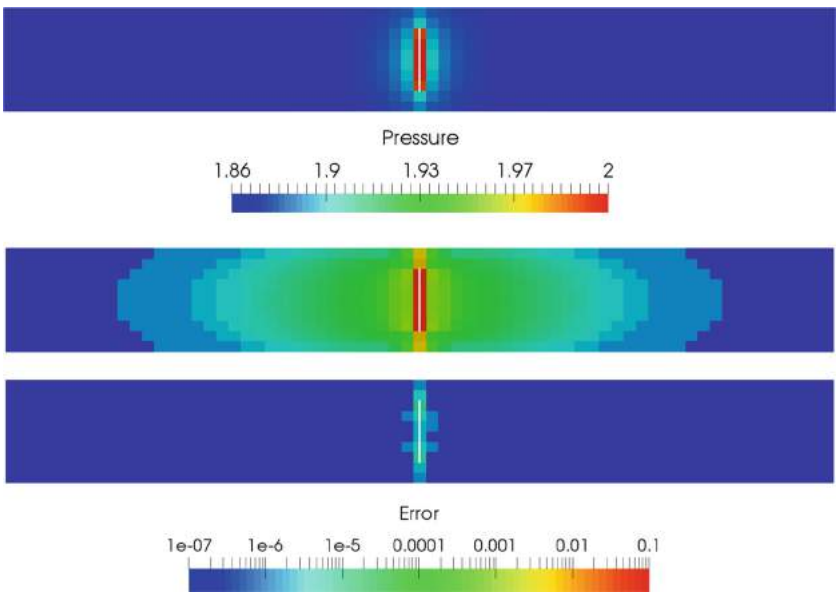

Fig. 10 Analytical solution (*top*) for the partially perforated well and solution error for the NFV (*middle*) and the NWC (*bottom*) methods

Table 6 Solution error for the NFV and the NWC methods for the partially perforated well case. Both schemes use the analytical flux to the well cells

N	$\varepsilon_{p,anl}^{NFV}$	$\varepsilon_{p,anl}^{NWC}$
33	1.0e–3	5.5e–10
67	4.4e–4	3.3e–8
99	2.6e–4	4.6e–9

well case. Errors for the NFV and the NWC methods are shown in Fig. 10 (middle and bottom). Both schemes use the analytical flux to the well cells proportional to the perforation size inside a cell. Table 6 contains solution errors for two methods.

5.5 2D isotropic case, two wells

The last experiment deals with two wells in the box domain. Domain dimensions are $[-100; 100] \times [-50; 50] \times [0; d]$. We consider the domain as pseudo-2D and neglect z coordinate in further description. The domain contains two vertical perfect wells located at $(-50, 0)$ and $(50, 0)$. The well rates are $q_1 = 1, q_2 = 4$. The permeability tensor is scalar, $\mathbb{K} = \mathbb{I}$.

The analytical solution for this problem is suggested in [8]:

$$p = \frac{q_1 \ln r_1}{2\pi k h_w} + \frac{q_2 \ln r_2}{2\pi k h_w} + C,$$

where h_w is the well height ($h_w = d = 3$ in our case), and C is some constant.

In order to fix a unique solution, we set the pressure in the middle point $\mathbf{x}_0 = (0, 0)$, $P_0 = p(\mathbf{x}_0) = 1.5$. The analytical solution then becomes (see Fig. 11):

$$p = P_0 - \frac{q_1 \ln (r_1/r_{w,p1})}{2\pi k h_w} + \frac{q_2 \ln (r_2/r_{w,p2})}{2\pi k h_w},$$

where r_1, r_2 are the distances from the current point to the wells 1 and 2, respectively, and $r_{w,p1}$, $r_{w,p2}$ are the distances from the middle point $\mathbf{x}_0$ to the wells. Pressures on the wells are obtained from this formula.

The radii of the near-well regions used in the logarithmic correction for both wells are $R_1 = R_2 = 30$.

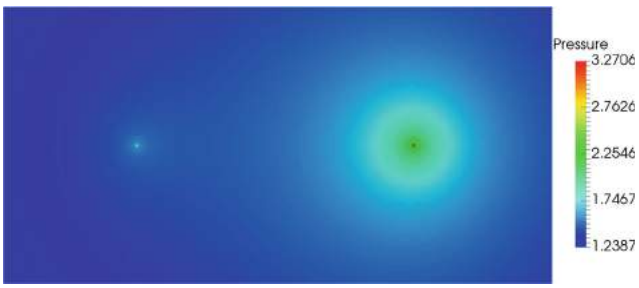

Fig. 11 Analytical solution for two wells problem

Table 7 Solution relative errors and flux errors for q_1 and q_2 for the problem with two wells for cubic grids

$100/h$	$\varepsilon_{p,anl}^{NFV}$	$\varepsilon_{p,anl}^{NWC}$	$\varepsilon_{p,pcm}^{NFV}$	ε_{p}^{NWC}
33	1.2e–2	2.8e–5	1.2e–2	2.8e–5
67	5.1e–3	7.0e–6	5.2e–3	7.6e–6
99	3.1e–3	3.2e–6	3.1e–3	4.1e–6
$100/h$	$\varepsilon_{q_1}^{NFV}$	$\varepsilon_{q_2}^{NFV}$	$\varepsilon_{q_1}^{NWC}$	$\varepsilon_{q_2}^{NWC}$
33	4.6e–3	1.9e–2	2.1e–5	4.1e–5
67	4.6e–3	1.9e–2	2.3e–5	5.4e–5
99	4.6e–3	1.8e–2	2.0e–5	7.0e–5

For the two wells case, we use the simplest cubic grids that are the best meshes for the Peaceman method. Grid dimensions are $66 \times 33 \times 1$, $134 \times 67 \times 1$ and $198 \times 99 \times 1$.

Table 7 shows the relative errors for the NFV and the NWC methods for the analytical well rates, relative errors for the pressure and the well rates (the first and the second well) for the numerical well models: NFV + Peaceman and the NWC method.

Figure 12 presents the error fields for the NFV scheme with the Peaceman well model and the NWC method in the *log*-scale. Note that the NFV scheme reduces to the standard FV scheme with the linear two-point flux approximation on cubic mesh and isotropic media. The largest error of the NFV scheme is concentrated in regions around the wells that are covered by the near-well regions of the NWC method. The NWC method gives considerably smaller errors than the conventional method.

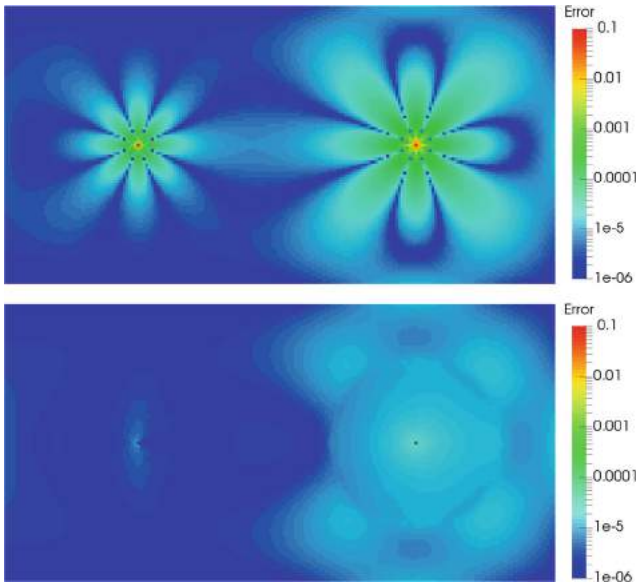

Fig. 12 Relative errors for the NFV scheme with Peaceman well model (*top*) and the NWC (*bottom*) methods in the *log*-scale. Cubic grid $134 \times 67 \times 1$

6 Discussions and conclusions

We presented the new near-well correction (NWC) method for the general case of anisotropic media, polyhedral grids, and arbitrarily oriented wells including slanted, shifted and partially perforated cases.

Numerical experiments show the noticeable improvement of accuracy compared to the original monotone nonlinear FV scheme with the conventional Peaceman well model or with the given analytical well rate. Practical implication of the improved accuracy is more accurate calculation of the well rates even on coarse grids.

We used the linear version of the method and achieved better accuracy compared to the nonlinear scheme by the cost of waiving the solution monotonicity in the near-well region. Choosing the nonlinear weights in (10) may help to retrieve additional properties of the solution such as monotonicity or preserving the DMP, which is the subject of future study.

The local grid refinement, which is widely used for modelling areas with high-pressure gradients, is not required in our approximation, since the NWC method provides enhanced accuracy for arbitrary well cells.

The study presented in this paper covers a single-phase flow; however, the approach can also be extended to the multiphase flows model. The construction of the method also allows us to consider more complex structures (e.g., wells with hydraulic fractures), as soon as we can compute local solution (analytical or numerical) for the flow generated by this structure.

Acknowledgments This work has been supported in part by RFBR grant 17-01-00886, Russian Federation President Grant MK-2951.2017.1, and ExxonMobil Upstream Research Company.

References

1. Bertolazzi, E., Manzini, G.: A second-order maximum principle preserving finite volume method for steady convection-diffusion problems. SIAM J. Numer. Anal. **43**(5), 2172–2199 (2005)
2. Chernyshenko, A., Vassilevski, Y.: A finite volume scheme with the discrete maximum principle for diffusion equations on polyhedral meshes. Finite Volumes for Complex Applications VII-Methods and Theoretical Aspects, 197–205 (2014)
3. Danilov, A., Vassilevski, Y.: A monotone nonlinear finite volume method for diffusion equations on conformal polyhedral meshes. Russ. J. Numer. Anal. Math. Model. **24**(3), 207–227 (2009)
4. Ding, Y., Jeannin, L.: A new methodology for singularity modelling in flow simulations in reservoir engineering (2001)
5. Dotlić, M., Vidović, D., Pokorni, B., Pušić, M., Dimkić, M.: Second-order accurate finite volume method for well-driven flows. J. Comp. Phys. **307**, 460–475 (2016)
6. Droniou, J.: Finite volume schemes for diffusion equations: introduction to and review of modern methods. Math. Models Methods Appl. Sci. **24**(8), 1575–1619 (2014)
7. Gao, Z.M., Wu, J.M.: A small stencil and extremum-preserving scheme for anisotropic diffusion problems on arbitrary 2D and 3D meshes. J. Comp. Phys. **250**, 308–331 (2013)
8. Haitjema, H.M.: Analytic element modeling of groundwater flow. ClassPak Publishing (2005)
9. LePotier, C.: Schema volumes finis monotone pour des operateurs de diffusion fortement anisotropes sur des maillages de triangle non structures. C. R. Acad. Sci. Paris, Ser. I **341**, 787–792 (2005)
10. Lipnikov, K., Moulton, D., Svyatskiy, D.: A multiscale multilevel mimetic (m3) method for well-driven flows in porous media. Procedia Comput. Sci. **1**(1), 771–779 (2010)
11. Lipnikov, K., Svyatskiy, D., Vassilevski, Y.: Interpolation-free monotone finite volume method for diffusion equations on polygonal meshes. J. Comp. Phys. **228**(3), 703–716 (2009)
12. Lipnikov, K., Svyatskiy, D., Vassilevski, Y.: A monotone finite volume method for advection-diffusion equations on unstructured polygonal meshes. J. Comp. Phys. **229**, 4017–4032 (2010)
13. Lipnikov, K., Svyatskiy, D., Vassilevski, Y.: Minimal stencil finite volume scheme with the discrete maximum principle. Russ. J. Numer. Anal. Math. Model. **27**(4), 369–385 (2012)
14. Nikitin, K., Novikov, K., Vassilevski, Y.: Nonlinear finite volume method with discrete maximum principle for the two-phase flow model. Lobachevskii J. Math. 37(4) (2016)
15. Nikitin, K., Terekhov, K., Vassilevski, Y.: A monotone nonlinear finite volume method for diffusion equations and multiphase flows. Comp. Geosci. **18**(3), 311–324 (2014). doi:10.1007/s10596-013-9387-6
16. Nikitin, K., Terekhov, K., Vassilevski, Y.: Multiphase flows – nonlinear monotone FV scheme and dynamic grids. ECMOR XIV (2014)
17. Nikitin, K., Vassilevski, Y.: A monotone nonlinear finite volume method for advection-diffusion equations on unstructured polyhedral meshes in 3D. Russ. J. Numer. Anal. Math. Model. **25**(4), 335–358 (2010)
18. Peaceman, D.W.: Interpretation of well-block pressures in numerical reservoir simulation. SPEJ **18**(3), 183–194 (1978)
19. Peaceman, D.W.: Interpretation of well-block pressures in numerical reservoir simulation with non-square grid blocks and anisotropic permeability. SPEJ **23**(3), 531–543 (1983)
20. Sheng, Z., Yuan, G.: The finite volume scheme preserving extremum principle for diffusion equations on polygonal meshes. J. Comp. Physiol. **230**(7), 2588–2604 (2011)
21. Terekhov, K., Vassilevski, Y.: Two-phase water flooding simulations on dynamic adaptive octree grids with two-point nonlinear fluxes. Russ. J. Numer. Anal. Math. Model. **28**(3), 267–288 (2013)